

RESEARCH ARTICLE

Open Access



# Molecular mechanisms underlying the neural correlates of working memory

Xiaotao Xu<sup>1,2,3,4†</sup>, Han Zhao<sup>1,2,3,4†</sup>, Yu Song<sup>1,2,3,4†</sup>, Huanhuan Cai<sup>1,2,3,4</sup>, Wenming Zhao<sup>1,2,3,4</sup>, Jin Tang<sup>1,5\*</sup>, Jiajia Zhu<sup>1,2,3,4\*</sup> and Yongqiang Yu<sup>1,2,3,4\*</sup>

## Abstract

**Background** Working memory (WM), a core component of executive functions, relies on a dedicated brain system that maintains and stores information in the short term. While extensive neuroimaging research has identified a distributed set of neural substrates relevant to WM, their underlying molecular mechanisms remain enigmatic. This study investigated the neural correlates of WM as well as their underlying molecular mechanisms.

**Results** Our voxel-wise analyses of resting-state functional MRI data from 502 healthy young adults showed that better WM performance (higher accuracy and shorter reaction time of the 3-back task) was associated with lower functional connectivity density (FCD) in the left inferior temporal gyrus and higher FCD in the left anterior cingulate cortex. A combination of transcriptome-neuroimaging spatial correlation and the ensemble-based gene category enrichment analysis revealed that the identified neural correlates of WM were associated with expression of diverse gene categories involving important cortical components and their biological processes as well as sodium channels. Cross-region spatial correlation analyses demonstrated significant associations between the neural correlates of WM and a range of neurotransmitters including dopamine, glutamate, serotonin, and acetylcholine.

**Conclusions** These findings may help to shed light on the molecular mechanisms underlying the neural correlates of WM.

**Keywords** Working memory, Functional MRI, Functional connectivity density, Gene expression, Neurotransmitter

## Background

Working memory (WM), a core component of executive functions [1], refers to temporary storage and manipulation of the information necessary for complex cognitive tasks [2]. WM relies on a dedicated brain system that maintains and stores information in the short term [3]. Considerable effort in the last decades has been directed to investigating such brain system using two different yet complementary neuroimaging approaches, focusing on within-subject effects and between-subject differences respectively. The former examines an individual's brain activation during WM tasks utilizing functional neuroimaging techniques and the activated brain regions are thought to be responsible for WM processes [4, 5]. The latter explores inter-individual variations in brain structure and function

<sup>†</sup>Xiaotao Xu, Han Zhao and Yu Song contributed equally to this work.

\*Correspondence:

Jin Tang

tangjin@ahu.edu.cn

Jiajia Zhu

zhujiagiagraduate@163.com

Yongqiang Yu

cj.yuyongqiang@vip.163.com

<sup>1</sup> Department of Radiology, The First Affiliated Hospital of Anhui Medical University, Hefei 230022, China

<sup>2</sup> Research Center of Clinical Medical Imaging, Anhui Province, Hefei 230032, China

<sup>3</sup> Anhui Provincial Institute of Translational Medicine, Hefei 230032, China

<sup>4</sup> Anhui Provincial Key Laboratory for Brain Bank Construction and Resource Utilization, Hefei 230032, China

<sup>5</sup> Institute of Artificial Intelligence, Hefei Comprehensive National Science Center, Hefei 230026, China



that are linked to inter-individual differences in WM performance by conducting neuroimaging-behavior correlation across subjects [6]. Taking advantage of these approaches, extensive research has identified a distributed set of neural substrates relevant to WM, consistently involving the medial and lateral prefrontal cortex, medial and lateral posterior parietal cortex, and anterior and posterior cingulate cortex [4, 5, 7–15]. Nevertheless, the molecular mechanisms (i.e., genetic architecture and neurochemical basis) underlying the neural correlates of WM remain enigmatic.

Resting-state functional magnetic resonance imaging (fMRI) technique has been widely adopted to assess the intrinsic functional architecture of the brain by examining spontaneous fluctuations in the blood-oxygen-level-dependent (BOLD) signal as a potentially important manifestation of spontaneous neuronal activity [16]. Broadly, resting-state fMRI measures can be categorized into local neural activity measures and functional connectivity (FC) measures. The former include amplitude of low-frequency fluctuations (ALFF), fractional amplitude of low-frequency fluctuations (fALFF), and regional homogeneity (ReHo), which describe the local functional features of a single region and cannot depict the relational characteristics between regions. Resting-state FC evaluates inter-regional correlations in spontaneous BOLD signal fluctuations [17] and has shown high reliability [18, 19] and heritability [20, 21]. Resting-state FC measures can be calculated using hypothesis-driven and data-driven approaches. Seed-based FC analysis represents a commonly used hypothesis-driven approach to mapping intrinsic brain connectivity networks [22–24]. Due to the fact that seed regions must be specified a priori, this method has lacked an independent view and thus may provide an incomplete picture of whole-brain FC profiling. Although data-driven independent component analysis (ICA) attempts to resolve the dependence on prior knowledge [25], it carries out subjective analysis of physiological signals and noises, which might lead to incorrect models and high residual errors. In contrast, functional connectivity density (FCD) has emerged as a reproducible data-driven, graph-theory method to construct whole-brain FC networks and analyze their nodal degree centrality at the voxel level [26–29], facilitating a better characterization of brain functional topological organization. Brain areas with higher FCD values are considered more densely interconnected hub regions that are of more importance for neural convergence and global information integration. The FCD method has been employed to identify abnormal functional hubs in neuropsychiatric disorders [30, 31] as well as the neural correlates of human cognitive domains including WM [32–34].

The recent introduction of comprehensive whole-brain gene expression atlases, such as the Allen Human Brain Atlas (AHBA) [35, 36], has given rise to the burgeoning field of imaging transcriptomics. Imaging transcriptomics is concerned with the identification of spatial correlations between gene expression patterns and neuroimaging phenotype profiles [37–48], commonly followed by further gene category enrichment analysis (GCEA) to determine the biological functions that contribute to such correlations with the use of gene-to-category annotation systems like the gene ontology (GO) [49]. However, traditional GCEA is often biased by gene co-expression and spatial auto-correlation. To address this concern, a flexible ensemble-based null model has recently been developed to enable more valid and interpretable inference of GCEA [50], which allows researchers to better investigate the genetic architecture of neuroimaging phenotypes. In parallel, the progress in nuclear imaging techniques and tracers has made it increasingly feasible to precisely and reliably quantify a set of neurotransmitter receptors and transporters across the whole brain [51–55]. These neurotransmitter atlases have offered us sufficient material to explore the neurochemical basis of brain structure and function [56]. Collectively, the current availability of brain-wide gene expression and neurotransmitter atlases along with the continuing methodological refinement could open new avenues to examine the spatial relations between these atlases and neuroimaging findings, which may yield an updated framework for understanding the potential molecular mechanisms underlying the neural correlates of WM.

Our purposes in the current work were twofold. Initially, we computed FCD using resting-state fMRI data to investigate their associations with WM performance as measured by a 3-back task across a large sample of 502 healthy young adults. Next, we investigated the spatial relations of the identified neural correlates of WM with gene expression and neurotransmitter atlases to examine their potential genetic architecture and neurochemical basis. Schematic representation of the research design and analytical procedure is provided in Fig. 1.

## Results

### Neural correlates of WM

Our voxel-wise analyses revealed significant correlations between WM and FCD across 502 healthy young adults ( $P < 0.05$ , cluster-level family-wise error [FWE] corrected). Specifically, there was a significant negative correlation between 3-back task accuracy and FCD in the left inferior temporal gyrus (cluster size = 91 voxels, peak Montreal Neurological Institute [MNI] coordinate:  $x = -48$ ,  $y = -15$ ,  $z = -36$ , peak  $t = -4.54$ , partial correlation coefficient [ $pr$ ] =  $-0.232$ ,  $P < 0.001$ ) (Fig. 2A). In

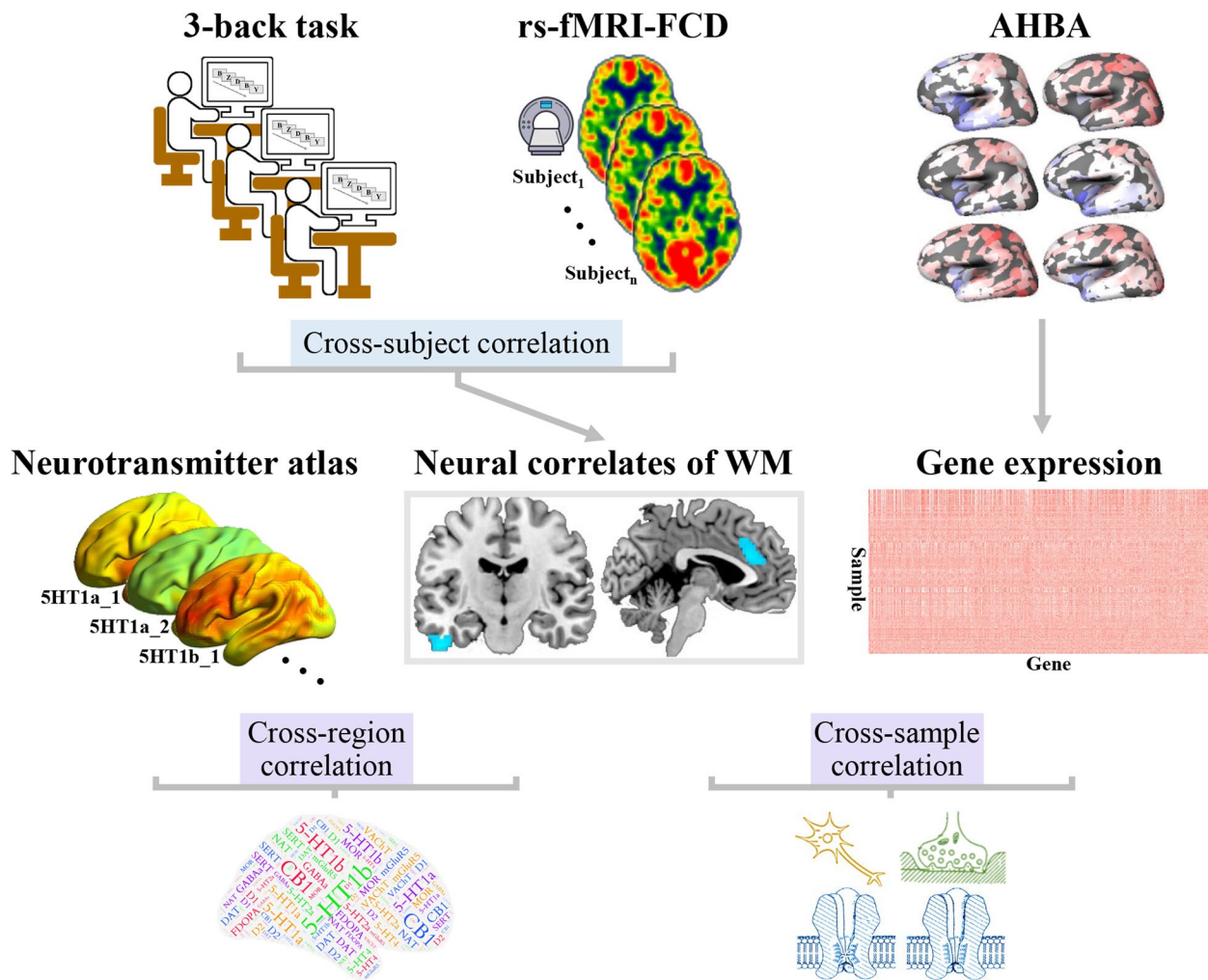


**Fig. 1** Research design and analytical procedure. Initially, we computed FCD using resting-state fMRI data to investigate their associations with WM performance as measured by a 3-back task across a large sample of 502 healthy young adults. Next, we investigated the spatial relations of the identified neural correlates of WM with gene expression and neurotransmitter atlases to examine their potential genetic architecture and neurochemical basis. Abbreviations: rs-fMRI, resting-state functional magnetic resonance imaging; FCD, functional connectivity density; AHBA, Allen Human Brain Atlas; WM, working memory

addition, we observed a significant negative correlation between 3-back task reaction time and FCD in the left anterior cingulate cortex (cluster size = 124 voxels, peak MNI coordinate:  $x = -3, y = 30, z = 24$ , peak  $t = -4.32$ ,  $pr = -0.211, P < 0.001$ ) (Fig. 2B).

**Gene categories associated with the neural correlates of WM**

A combination of transcriptome-neuroimaging spatial correlation and the ensemble-based GCEA revealed that the neural correlates of WM were spatially associated with gene expression of diverse GO categories (Additional file 1: Table S1). Briefly, the neural correlates of 3-back task accuracy were mainly associated

with ensheathment of neurons, axon ensheathment, axonogenesis, myelination, and sodium channel activity (Fig. 3A). The neural correlates of 3-back task reaction time were predominantly associated with neuron differentiation, postsynaptic signal transduction, regulation of neurotransmitter levels, presynapse, GABAergic synapse, ion channel complex, and channel activity (Fig. 3B).

**Neurotransmitters associated with the neural correlates of WM**

Cross-region spatial correlation analyses demonstrated significant associations between the neural correlates of WM and specific neurotransmitters (permutation-based

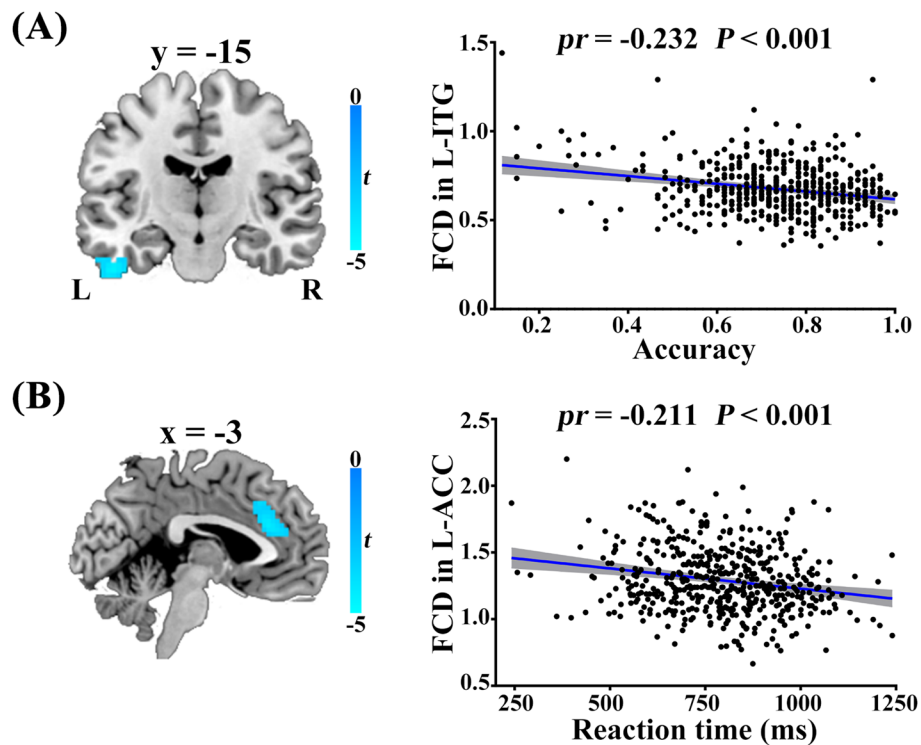


**Fig. 2** Neural correlates of working memory. Correlations of FCD with 3-back task accuracy (A) and reaction time (B) across 502 healthy young adults. Left panel: brain regions with FCD in relation to 3-back task performance. Right panel: scatter plots of the corresponding correlations. Abbreviations: FCD, functional connectivity density; ITG, inferior temporal gyrus; ACC, anterior cingulate cortex; L, left; R, right

$P < 0.05$ , Bonferroni corrected). Briefly, the neural correlates of 3-back task accuracy were positively associated with dopamine (D2\_2:  $r = 0.267$ ,  $P = 4 \times 10^{-4}$ ) (Fig. 4A and Additional file 2: Table S2). The neural correlates of 3-back task reaction time were positively associated with glutamate (mGluR5\_3:  $r = 0.337$ ,  $P = 1 \times 10^{-3}$ ), and negatively associated with dopamine (D2\_2:  $r = -0.294$ ,  $P = 2 \times 10^{-4}$ ), serotonin (SERT\_3:  $r = -0.354$ ,  $P = 2 \times 10^{-4}$ ) and acetylcholine (VAcHT\_3:  $r = -0.235$ ,  $P = 1.2 \times 10^{-3}$ ) (Fig. 4B and Additional file 3: Table S3).

**Sensitivity analysis**

To determine the effect of different differential stability (DS, a measure of consistent regional variation across donor brains) threshold selections, we used two other DS cutoff thresholds (top 40% and 60%) during the brain gene expression data processing to obtain normalized expression measures of 4010 and 6016 genes, respectively. By repeating the transcriptome-neuroimaging spatial correlation and the ensemble-based GCEA, we found substantial overlaps between the GO categories identified in the main and sensitivity analyses, with 40% corresponding to Additional File 4: Table S4 and 60% to Additional File 5: Table S5.

**Discussion**

This study investigated the neural correlates of WM using resting-state fMRI data from a large sample of healthy young adults, as well as their underlying molecular mechanisms using spatial correlations with gene expression and neurotransmitter atlases. Our data showed that better WM performance (higher accuracy and shorter reaction time of the 3-back task) was correlated with lower FCD in the left inferior temporal gyrus and higher FCD in the left anterior cingulate cortex. A combination of transcriptome-neuroimaging spatial correlation and the ensemble-based GCEA revealed that the identified neural correlates of WM were spatially associated with gene expression of diverse GO categories involving important cortical components and their biological processes as well as sodium channels. Cross-region spatial correlation analyses demonstrated significant associations between the neural correlates of WM and a range of neurotransmitters including dopamine, glutamate, serotonin, and acetylcholine. These findings are crucial not only for unraveling the mechanisms underlying WM processes but also for gaining insights into disorders characterized by WM deficits, such as attention deficit hyperactivity disorder, Alzheimer’s disease, and schizophrenia.

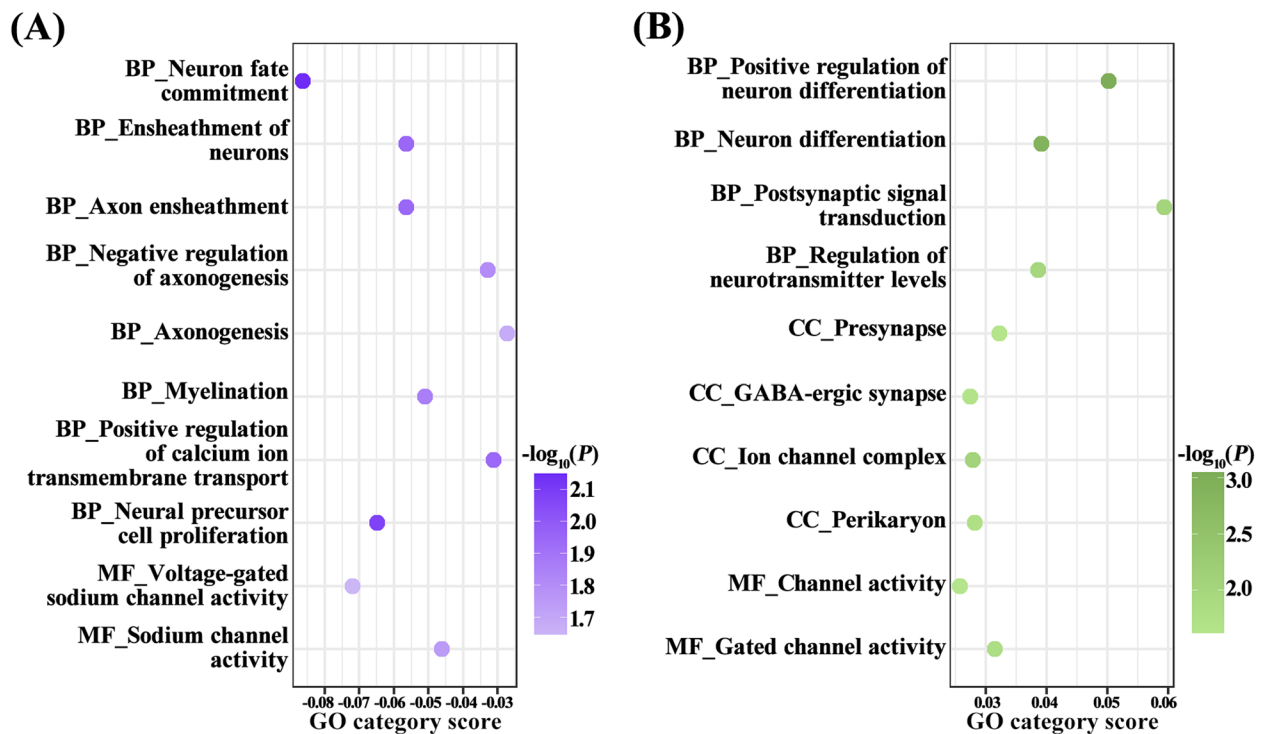


**Fig. 3** Gene categories associated with the neural correlates of working memory. A combination of transcriptome-neuroimaging spatial correlation and the ensemble-based GCEA revealed that the neural correlates of 3-back task accuracy **(A)** and reaction time **(B)** were spatially associated with gene expression of diverse GO categories. Abbreviations: GCEA, gene category enrichment analysis; GO, gene ontology; BP, biological process; MF, molecular function; CC, cellular component

We found that 3-back task accuracy and reaction time were negatively correlated with FCD in the inferior temporal gyrus and anterior cingulate cortex respectively, indicating that better WM performance (higher accuracy and shorter reaction time) may rely on lower FCD in the inferior temporal gyrus and higher FCD in the anterior cingulate cortex. Previous functional neuroimaging meta-analyses have suggested WM task-evoked brain activation in a fronto-cingulo-parietal cognitive control network [9, 10]. Our observation of a link between better WM performance and higher FCD in the anterior cingulate cortex is congruent with these prior findings, raising the possibility that increased nodal centrality of the anterior cingulate cortex may reflect its strengthened role in coordinating the fronto-cingulo-parietal cognitive control network in response to WM tasks. It seems counter-intuitive that we observed an association between better WM performance and lower FCD in the inferior temporal gyrus that is outside the fronto-cingulo-parietal network. However, it is likely that brain regions contributing to individual differences in WM are not necessarily those that are directly implicated in WM processes. The inferior temporal gyrus has been frequently known to be involved in multiple cognitive functions including WM

[57–60]. Although speculative, a potential explanation is that lower resting-state intrinsic activity in the inferior temporal gyrus can increase its ability to be recruited according to WM task demands, resulting in better performance. An alternative explanation is that lower FCD in the inferior temporal gyrus may be an epiphenomenon rather than a cause of better WM performance, i.e., more efficient communication and coordination in the fronto-cingulo-parietal network may come at the cost of reduced neural activity in regions outside this network. It is noteworthy that the identified neural correlates of WM were left-lateralized. This hemispheric lateralization is compatible with findings from many prior studies [61–65]. One possible explanation may be that the information being remembered in verbal WM tasks is language-related and thus there is a left-hemisphere dominance in the specific neural processes involved.

A combination of transcriptome-neuroimaging spatial correlation and the ensemble-based GCEA revealed that the neural correlates of WM were spatially associated with gene expression of diverse GO categories involving important cortical components and their biological processes as well as sodium channels. Neurons, axons, and synapses are important cortical components. These

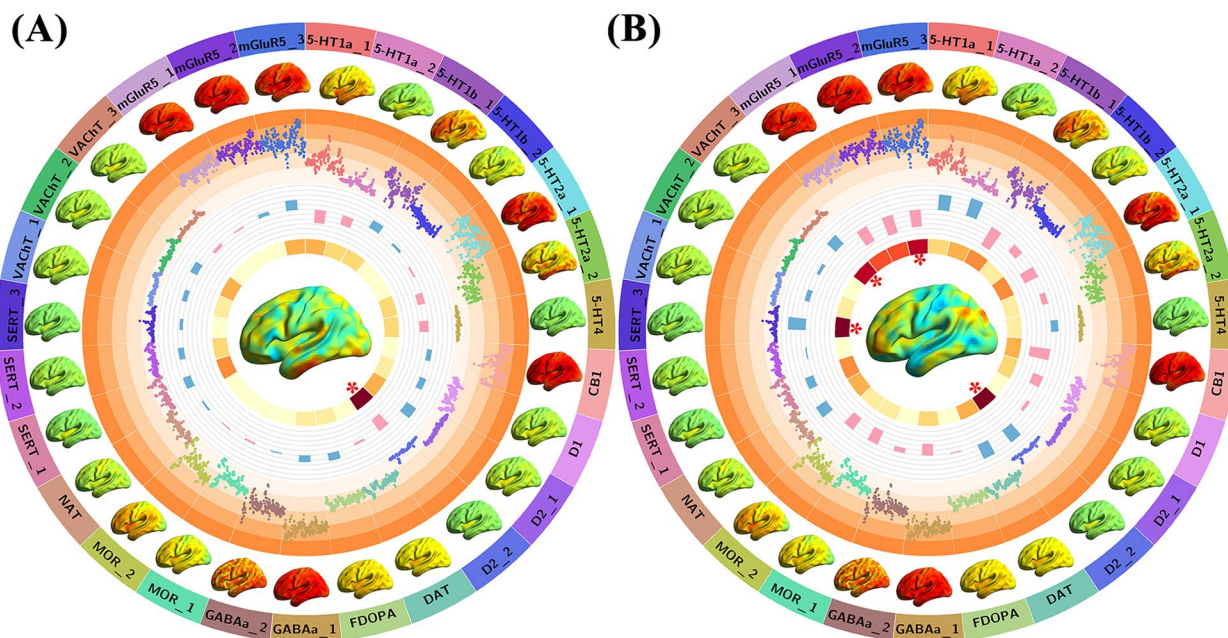


**Fig. 4** Neurotransmitters associated with the neural correlates of working memory. Cross-region spatial correlations of neurotransmitters with the neural correlates of 3-back task accuracy (A) and reaction time (B). The outermost ring shows the names and maps of 27 neurotransmitter receptors/transporters. The second circle displays the neurotransmitter values across 210 cerebral cortical regions derived from the Human Brainnetome Atlas. The third circle displays the cross-region Pearson's correlation coefficients between these neurotransmitter maps and the neural correlates of working memory, with the red (blue) color indicating the positive (negative) correlation coefficients and the column height indicating the magnitude of correlation coefficients. The innermost ring displays the permutation-based statistical significance of the spatial correlations, i.e.,  $-\log_{10}(P)$ , with the darker color indicating the lower  $P$  value; \* $P < 0.05$ , Bonferroni corrected. The  $t$  maps for the correlations between FCD and working memory performance lie in the center. Abbreviations: 5-HT, 5-hydroxytryptamine; CB1, cannabinoid type 1; D, dopamine; DAT, dopamine transporter; FDOPA, fluorodopa; GABAa, gamma-aminobutyric acid a; MOR, mu opioid receptor; NAT, noradrenaline transporter; SERT, serotonin transporter; VACHT, vesicular acetylcholine transporter; mGluR5, metabotropic glutamate type 5; FCD, functional connectivity density

cortical components and their biological processes (e.g., ensheathment of neurons and axons, axonogenesis, myelination, neuron differentiation, and postsynaptic signal transduction) have been associated with WM [66–77]. Voltage-gated sodium channels are responsible for the generation and propagation of the action potential [78]. Lamotrigine, a use-dependent inhibitor of voltage-gated sodium channels, has been shown to enhance cortical function within the neural circuits subserving WM in patients with bipolar disorder [79], providing indirect evidence for the relation between WM and sodium channels. In addition, the identified GO categories included neurotransmitters, which echoes the following spatial correlation results with neurotransmitter atlases.

Cross-region spatial correlation analyses demonstrated significant associations between the neural correlates of WM and a range of neurotransmitters including dopamine, glutamate, serotonin, and acetylcholine. It is noteworthy that earlier literature has attempted to establish the links between rs-fMRI measures and neurotransmitters using invasive techniques such as positron emission tomography. Benefiting from publicly available

neurotransmitter atlases, we could explore such links in a non-invasive way. The involvement of the dopamine system in WM processes is well acknowledged [80–84]. Animal research has shown that mice lacking dopamine receptors exhibit spatial WM deficits [85]. The metabotropic glutamate receptors (mGluRs) are family C G-protein-coupled receptors that participate in the modulation of synaptic transmission and neuronal excitability throughout the brain [86]. Prior work has demonstrated effects of blocking mGluR5 on dorsolateral prefrontal cortical neuronal firing and WM performance [87]. The serotonin system derives mainly from neurons in the dorsal and ventral raphe nuclei with projections to virtually every brain region that subserves cognition. It is generally accepted that serotonin receptors are engaged in learning and memory, and represent highly favorable molecular targets for cognitive enhancement in disorders [88, 89]. There is solid evidence that acetylcholine receptors play a critical role in facilitating cognitive processes including WM, and cholinergic dysfunction has been associated with cognitive abnormalities in a variety of neurodegenerative and neuropsychiatric diseases

[90–93]. Combined, our findings, taken with the previous reports, support the notion that WM is a complex cognitive function entailing multiple neurotransmitter systems that may work independently or synergistically with each other.

Several limitations are worth mentioning in the present study. First, given that our study sample was a group of educated healthy young adults, these findings might not be representative of the general population. Further investigations in participants with broader age and education ranges are needed to validate our results. Second, we did not perform distortion corrections during the preprocessing of fMRI data, which may have an impact on the BOLD signal. Third, it is not possible to make strong inferences regarding the direction of causality due to the correlative nature of the analyses. Fourth, our transcriptome-neuroimaging spatial correlation analyses only considered the tissue samples in the left cerebral cortex because of limited gene expression data in the right hemisphere and different gene expression profiles between cortical and subcortical regions. The reduced tissue samples along with hemisphere and region selections might introduce potential biases. Finally, the neural correlates of WM were derived from our resting-state fMRI data, while the gene expression and neurotransmitter atlases were obtained from publicly available datasets. Differences across individuals were ignored during the spatial correlation analyses, which may influence our interpretation.

## Conclusions

In conclusion, our work demonstrated that better WM performance was correlated with hypoconnectivity in the inferior temporal gyrus and hyperconnectivity in the anterior cingulate cortex. Furthermore, these neural correlates of WM were potentially modulated by specific genetic architecture and neurochemical basis. Our findings may help to shed light on the molecular mechanisms underlying the neural correlates of WM.

## Methods

### Participants

A total of 502 healthy young adults were recruited by advertisement. All participants met the inclusion criteria of Chinese Han, right-handedness, and within a restricted age range of 18–30 years, which corresponds to a period after the completion of major neurodevelopment and before the onset of neurodegeneration. Exclusion criteria included neuropsychiatric or serious somatic disorders, a history of alcohol or drug abuse, regular smoking (i.e., total number of cigarettes > 20), current medication (e.g., sedative-hypnotics) within a month, pregnancy, MRI contraindications, and a family

history of psychiatric illness among first-degree relatives. The MINI-International Neuropsychiatric Interview (M.I.N.I.) and Alcohol Use Disorders Identification Test (AUDIT) were used in the process of excluding participants. This study was conducted in accordance with the Declaration of Helsinki and was approved by the ethics committee of The First Affiliated Hospital of Anhui Medical University (20200094). Written informed consent was obtained from all participants after they had been given a complete description of the study. Detailed data of the sample are listed in Table 1.

### Working memory assessment

The letter 3-back task was conducted on a computer to assess WM [9] using E-Prime 2.0 [94]. During the task, each participant viewed a series of letters that were presented sequentially and the presentation time of each letter stimulus was 200 ms with an inter-stimulus interval of 1800 ms. Participants were instructed to press a button on the right with their middle fingers if the letter that appeared on the screen was identical to the one presented 3 letters earlier, and otherwise to press a button on the left with their index fingers. The task consisted of 60 trials. Before the formal test, participants were verbally instructed and had a practice test to ensure that they understood the task. The accuracy and mean reaction time of correct responses were used as the indices of WM performance.

### MRI data acquisition

MRI scans were obtained using a 3.0-Tesla MR system (Discovery MR750w, General Electric, Milwaukee, WI, USA) with a 24-channel head coil. Earplugs were used to reduce scanner noise, and tight but comfortable foam padding was used to minimize head motion. High-resolution 3D T1-weighted structural images were acquired by employing a brain volume (BRAVO) sequence with the following parameters: repetition time (TR) = 8.5 ms; echo time (TE) = 3.2 ms; inversion time (TI) = 450 ms; flip

**Table 1** Demographic and cognitive characteristics of the participants

Characteristic	Mean ± SD	Range
Sex (female/male)	314/188	-
Age (years)	23.28 ± 2.44	18–30
Education (years)	16.66 ± 1.81	12–22
3-back task performance		
Accuracy	0.73 ± 0.15	0.12–1.00
Reaction time (ms)	795.65 ± 162.22	241.44–1240.52
FD (mm)	0.11 ± 0.05	0.04–0.40

Abbreviations: SD Standard deviation; FD Frame-wise displacement

angle (FA) = 12°, field of view (FOV) = 256 mm × 256 mm; matrix size = 256 × 256; slice thickness = 1 mm, no gap; 188 sagittal slices; and acquisition time = 296 s. Resting-state BOLD fMRI data were acquired using a gradient-echo single-shot echo planar imaging (GRE-SS-EPI) sequence with the following parameters: TR = 2000 ms; TE = 30 ms; FA = 90°; FOV = 220 mm × 220 mm; matrix size = 64 × 64; slice thickness = 3 mm, slice gap = 1 mm; 35 interleaved axial slices; 185 volumes; and acquisition time = 370 s. Before the scanning, all subjects were instructed to keep their eyes closed, relax, move as little as possible, think of nothing in particular, and not fall asleep during the scans. During and after the scanning, we asked subjects whether they had fallen asleep to confirm that none of them had done so. All MR images were visually inspected to ensure that only images without visible artifacts were included in subsequent analyses.

#### fMRI data preprocessing

Resting-state BOLD data were preprocessed using Statistical Parametric Mapping (SPM12) [95] and Data Processing & Analysis for Brain Imaging (DPABI) [96, 97]. The first 10 volumes for each participant were discarded to allow the signal to reach equilibrium and the participants to adapt to the scanning noise. The remaining volumes were corrected for the acquisition time delay between slices. Then, realignment was performed to correct the motion between time points. Head motion parameters were computed by estimating the translation in each direction and the angular rotation on each axis for each volume. All participants' BOLD data were within the defined motion thresholds (i.e., translational or rotational motion parameters less than 2 mm or 2°). We also calculated frame-wise displacement (FD), which indexes the volume-to-volume changes in head position. Several nuisance covariates (the linear drift, the estimated motion parameters based on the Friston-24 model, the spike volumes with  $FD > 0.5$  mm, the white matter signal, and the cerebrospinal fluid signal) were regressed out from the data. Notably, we did not perform global signal regression since it is still a controversial topic in resting-state fMRI analysis [98]. The datasets were then band-pass filtered using a frequency range of 0.01–0.1 Hz. In the normalization step, individual structural images were firstly co-registered with the mean functional images; then the transformed structural images were segmented and normalized to the MNI space using a high-level nonlinear warping algorithm, that is, the diffeomorphic anatomical registration through the exponentiated Lie algebra (DARTEL) technique [99]. Finally, each filtered functional volume was spatially normalized to MNI space using the deformation parameters estimated during the above step and resampled into a 3-mm cubic voxel.

#### Functional connectivity density analysis

FCD was computed according to the method described by previous studies [26, 31, 100–102]. Pearson's correlation coefficients were calculated between the BOLD time courses of all pairs of voxels and a whole-brain functional connectivity matrix was obtained for each participant. For a given voxel, FCD was defined as the number of functional connections with correlation coefficients above a threshold of 0.25 between that voxel and all other voxels within the whole brain. This threshold was chosen because it effectively filters out noise and weak connections while preserving significant ones, thereby enhancing the accuracy and reliability of the FCD analysis [31, 34, 103–105]. Then, we normalized the FCD value of each voxel by dividing it by the global mean FCD value. The resultant FCD maps were spatially smoothed with a 6 mm full-width at half maximum Gaussian kernel.

#### Correlation between WM and FCD

A voxel-wise approach was used to examine the correlations between WM and FCD across 502 healthy young adults. We used multiple regression model implemented in the SPM12 to identify any voxels in the FCD images that showed significant correlations with 3-back task performance (accuracy and reaction time) while controlling for potential confounders including age, sex, education, and FD. The statistical analysis yielded a *t* map, representing the correlations between WM and FCD. For the voxel-based analysis, multiple comparison correction was performed using the cluster-level FWE method, resulting in a cluster-defining threshold of  $P = 0.001$  and a corrected cluster significance of  $P < 0.05$ .

#### Brain gene expression data processing

Brain gene expression data were acquired from the AHBA dataset [35, 106], which consists of six human post-mortem brains (Additional file 6: Table S6). The original expression data of more than 20,000 genes at 3702 spatially distinct brain tissue samples were processed following a newly proposed pipeline [37]. First, we updated the probe-to-gene annotations based on the latest information from the National Center for Biotechnology Information (NCBI) by means of the Re-Annotator toolkit [107]. Second, signal intensity filtration was conducted to exclude probes with signal intensity lower than background noise in at least 50% of the samples across all donors. Third, RNA-seq data were used to select the single probe that can represent each gene. Specifically, after excluding genes without RNA-seq measured expression values, we calculated Spearman's correlations between microarray and RNA-seq measures. We set a threshold of  $r > 0.2$  to select brain-relevant and reliably measured genes in accordance with current guidelines [37] in prior

studies [39, 41, 47, 48, 108]. Next, the probe with the highest correlation to RNA-seq data was selected as the representative probe for a gene. Fourth, considering the limited number of tissue samples in the right hemisphere (only two donors) and substantial differences in expression patterns between cortical and subcortical regions, we focused our analysis on the left cerebral cortex [109]. Fifth, scaled robust sigmoid normalization was performed at the within-sample cross-gene and within-gene cross-sample levels to correct for donor-specific effects. Finally, genes with the top 50% highest DS were selected for the subsequent analysis. For one, prior research has reported that genes with higher DS demonstrate more conserved expression patterns and are enriched for brain-related biological functions [110]. For another, gene expression conservation across subjects is a prerequisite for transcriptome-neuroimaging spatial correlation analysis. After these processing procedures, we obtained normalized expression data of 5013 genes for 1280 tissue samples. Since our WM-FCD correlation analysis was performed within a gray matter mask derived from the Human Brainnetome Atlas [111], we further restricted our analyses to the samples within this mask, resulting in a final sample  $\times$  gene matrix of  $623 \times 5013$ .

### Correlation with gene expression

We employed transcriptome-neuroimaging spatial correlation and the newly developed ensemble-based GCEA to explore the genetic architecture underlying the neural correlates of WM. Specifically, we drew a spherical region (radius = 3 mm) centered at the MNI coordinate of a given brain tissue sample and extracted the average  $t$ -value of voxels within the sphere from the statistical  $t$  maps for the WM-FCD correlations. Then, Pearson's correlation between gene expression and  $t$ -values across tissue samples was calculated in a gene-wise manner, yielding 5013 spatial correlation coefficients (henceforth referred to as gene scores). According to the Fulcher et al. study [50], we conducted neuroimaging-spatial ensemble-based GCEA for these gene scores in the following way. First, updated GO term hierarchy and annotation files were obtained from the GO [112] on 11th July 2022. Second, direct gene-to-category annotations were performed for the 5013 AHBA genes, and we restricted our analyses to GO categories with 10–200 annotations. Third, the gene scores were agglomerated at the level of GO categories as a mean score of genes annotated to each GO category. Fourth, 10,000 surrogate maps with spatial autocorrelation matching the  $t$  maps were generated using the BrainSMASH package [113], based on the spatial-lag model [114]. Null distributions (i.e., neuroimaging-spatial ensemble-based null model) of mean gene scores for each GO category were generated

through spatial correlations between gene expression and the 10,000 spatial autocorrelation-preserving surrogate maps. Finally, statistical significance of a GO category was assessed by comparing the GO category score derived from the real data to the neuroimaging-spatial ensemble-based null. The significance threshold was set at two-sided  $P < 0.05$  (i.e., higher or lower than the null).

### Correlation with neurotransmitters

JuSpace is a useful tool allowing for spatial correlation analyses between cross-modal neuroimaging data [115, 116]. To determine the neurochemical basis underlying the neural correlates of WM, we employed JuSpace to examine the spatial correlations of the  $t$  maps with nuclear imaging-derived measures covering various neurotransmitter systems including dopamine, serotonin, glutamate, gamma-aminobutyric acid (GABA), acetylcholine, opioid, cannabinoid, noradrenaline, and fluorodopa (Additional file 7: Table S7) [51, 117–131]. Specifically, Pearson's correlation coefficients between the  $t$  map and these neurotransmitter maps were computed across 210 cerebral cortical regions derived from the Human Brainnetome Atlas while adjusting for spatial autocorrelation and partial volume with the gray matter probability map. Exact  $P$  values were computed using spatial permutation-based null maps with 5000 permutations. Multiple comparisons were corrected using the Bonferroni method and a corrected  $P < 0.05$  was considered significant.

### Sensitivity analysis

We chose the genes with the top 50% highest DS to focus our analyses on genes with relatively more conserved expression patterns across six donors in the main analysis. Considering the possible impact of different DS thresholds, we repeated our analysis using two other DS cutoff thresholds (top 40% and 60%).

### Abbreviations

5-HT	5-Hydroxytryptamine
ACC	Anterior cingulate cortex
AHBA	Allen Human Brain Atlas
ALFF	Amplitude of low-frequency fluctuations
AUDIT	Alcohol Use Disorders Identification Test
BOLD	Blood-oxygen-level-dependent
BP	Biological process
BRAVO	Brain volume
CB1	Cannabinoid type 1
CC	Cellular component
D	Dopamine
DARTEL	Diffeomorphic anatomical registration through the exponentiated Lie algebra
DAT	Dopamine transporter
DPABI	Data Processing & Analysis for Brain Imaging
DS	Differential stability
FA	Flip angle
FC	Functional connectivity
FCD	Functional connectivity density

FD	Frame-wise displacement
FDOPA	Fluorodopa
FOV	Field of view
FWE	Family-wise error
GABA	Gamma-aminobutyric acid
GABAA	Gamma-aminobutyric acid a
GCEA	Gene category enrichment analysis
GO	Gene ontology
GRE-SS-EPI	Gradient-echo single-shot echo planar imaging
ICA	Independent component analysis
ITG	Inferior temporal gyrus
L	Left
M.I.N.I.	MINI-International Neuropsychiatric Interview
MF	Molecular function
MNI	Montreal Neurological Institute
MOR	Mu opioid receptor
NAT	Noradrenaline transporter
NCBI	National Center for Biotechnology Information
PET	Positron emission tomography
R	Right
ReHo	Regional homogeneity
SD	Standard deviation
SERT	Serotonin transporter
SPECT	Single photon emission computed tomography
SPM	Statistical Parametric Mapping
TE	Echo time
TI	Inversion time
TR	Repetition time
VAcHT	Vesicular acetylcholine transporter
WM	Working memory
fALFF	Fractional amplitude of low-frequency fluctuations
fMRI	Resting-state functional magnetic resonance imaging
mGluR5	Metabotropic glutamate type 5
mGluRs	Metabotropic glutamate receptors
<i>pr</i>	Partial correlation coefficient
rs-fMRI	Resting-state functional magnetic resonance imaging

## Supplementary Information

The online version contains supplementary material available at <https://doi.org/10.1186/s12915-024-02039-0>.

Additional file 1: Table S1. Gene categories associated with the neural correlates of working memory. This table presents all gene categories linked to the neural correlates of working memory at a threshold of 0.5. The sheet labeled "Accuracy" features the GO categories related to the neural correlates of 3-back task accuracy, while the "Reaction time" sheet includes the GO categories associated with the neural correlates of 3-back task reaction time. Available in.xls format.

Additional file 2: Table S2. Spatial associations between the neural correlates of 3-back task accuracy and neurotransmitters. This table outlines associations between the neural correlates of 3-back task accuracy and specific neurotransmitters. Available in.doc format.

Additional file 3: Table S3. Spatial associations between the neural correlates of 3-back task reaction time and neurotransmitters. This table outlines associations between the neural correlates of 3-back task reaction time and specific neurotransmitters. Available in.doc format.

Additional file 4: Table S4. Gene categories associated with the neural correlates of working memory at threshold 0.4. This table presents all gene categories linked to the neural correlates of working memory at a threshold of 0.4. The sheet labeled "Accuracy" features the GO categories related to the neural correlates of 3-back task accuracy, while the "Reaction time" sheet includes the GO categories associated with the neural correlates of 3-back task reaction time. Available in.xls format.

Additional file 5: Table S5. Gene categories associated with the neural correlates of working memory at a threshold of 0.6. This table presents all gene categories linked to the neural correlates of working memory at a threshold of 0.6. The sheet labeled "Accuracy" features the GO categories

related to the neural correlates of 3-back task accuracy, while the "Reaction time" sheet includes the GO categories associated with the neural correlates of 3-back task reaction time. Available in.xls format.

Additional file 6: Table S6. Demographic information of the six adult donors in the AHBA. This table provides the demographic information of six adult donors in the AHBA. Available in.doc format.

Additional file 7: Table S7. Receptor/transporter maps. This table shows the foundational information of all neurotransmitter maps provided by JuSpace. Available in.doc format.

## Acknowledgements

We thank the Allen Institute for Brain Science founders and staff who supplied the brain expression data. We also thank the subjects who contributed to this study.

## Authors' contributions

XX.: conceptualization, methodology, software, formal analysis, investigation, data curation, visualization, writing—original draft. H.Z.: methodology, software, validation, investigation, data curation. Y.S.: methodology, software, validation, investigation, data curation. H.C.: software, validation, formal analysis, data curation. W.Z.: methodology, formal analysis, writing—original draft. J.T.: conceptualization, methodology, validation, resources, supervision, project administration. J.Z.: conceptualization, methodology, validation, resources, writing—review and editing, supervision, project administration. Y.Y.: conceptualization, methodology, validation, resources, writing—review and editing, supervision, funding acquisition. All authors read and approved the final manuscript.

## Funding

This work was supported by the National Natural Science Foundation of China (grant numbers: 82471952, 82371928, and 82071905), the Anhui Provincial Natural Science Foundation (grant number: 2308085MH277), the Scientific Research Key Project of Anhui Province Universities (grant number: 2022AH051135), the Scientific Research Foundation of Anhui Medical University (grant number: 2022xkj143), and the Postgraduate Innovation Research and Practice Program of Anhui Medical University (grant number: YJS20230012).

## Data availability

All data generated or analyzed during this study are included in this published article, its supplementary information files, and publicly available repositories. We have submitted the resting-state fMRI data and the code to the Open Science Framework repository, where they are available for free access [132]. Brain gene expression data can be acquired from the AHBA dataset [35, 106] and the data for each brain are now available for download at <https://human.brain-map.org/static/download> under an open access mandate. Neurotransmitter atlases can be obtained from JuSpace [115, 116].

## Declarations

### Ethics approval and consent to participate

This study was conducted in accordance with the Declaration of Helsinki and was approved by the ethics committee of The First Affiliated Hospital of Anhui Medical University (20200094). Written informed consent was obtained from all participants after they had been given a complete description of the study.

### Consent for publication

Not applicable.

### Competing interests

The authors declare that they have no competing interests.

Received: 14 October 2023 Accepted: 11 October 2024  
Published online: 21 October 2024

## References

- Diamond A. Executive functions. *Annu Rev Psychol.* 2013;64:135–68.
- Baddeley A. Working memory. *Science.* 1992;255(5044):556–9.
- Baddeley A. Working memory: looking back and looking forward. *Nat Rev Neurosci.* 2003;4(10):829–39.
- Veltman DJ, Rombouts SA, Dolan RJ. Maintenance versus manipulation in verbal working memory revisited: an fMRI study. *Neuroimage.* 2003;18(2):247–56.
- Van Snellenberg JX, Slifstein M, Read C, Weber J, Thompson JL, Wager TD, et al. Dynamic shifts in brain network activation during supracapacity working memory task performance. *Hum Brain Mapp.* 2015;36(4):1245–64.
- Braver TS, Cole MW, Yarkoni T. Vive les differences! Individual variation in neural mechanisms of executive control. *Curr Opin Neurobiol.* 2010;20(2):242–50.
- van Dam WO, Decker SL, Durbin JS, Vendemia JM, Desai RH. Resting state signatures of domain and demand-specific working memory performance. *Neuroimage.* 2015;118:174–82.
- Zou Q, Ross TJ, Gu H, Geng X, Zuo XN, Hong LE, et al. Intrinsic resting-state activity predicts working memory brain activation and behavioral performance. *Hum Brain Mapp.* 2013;34(12):3204–15.
- Owen AM, McMillan KM, Laird AR, Bullmore E. N-back working memory paradigm: a meta-analysis of normative functional neuroimaging studies. *Hum Brain Mapp.* 2005;25(1):46–59.
- Niendam TA, Laird AR, Ray KL, Dean YM, Glahn DC, Carter CS. Meta-analytic evidence for a superordinate cognitive control network subserving diverse executive functions. *Cogn Affect Behav Neurosci.* 2012;12(2):241–68.
- Piras F, Caltagirone C, Spalletta G. Working memory performance and thalamus microstructure in healthy subjects. *Neuroscience.* 2010;171(2):496–505.
- Hampson M, Driesen NR, Skudlarski P, Gore JC, Constable RT. Brain connectivity related to working memory performance. *J Neurosci.* 2006;26(51):13338–43.
- Sala-Llonch R, Pena-Gomez C, Arenaza-Urquijo EM, Vidal-Pineiro D, Bargallo N, Junque C, et al. Brain connectivity during resting state and subsequent working memory task predicts behavioural performance. *Cortex.* 2012;48(9):1187–96.
- Zhang Y, Ji W, Jiang F, Wu F, Li G, Hu Y, et al. Associations among body mass index, working memory performance, gray matter volume, and brain activation in healthy children. *Cereb Cortex.* 2023;33(10):6335–44.
- Goghari VM, Macdonald AW 3rd, Sponheim SR. Relationship between prefrontal gray matter volumes and working memory performance in schizophrenia: a family study. *Schizophr Res.* 2014;153(1–3):113–21.
- Fox MD, Raichle ME. Spontaneous fluctuations in brain activity observed with functional magnetic resonance imaging. *Nat Rev Neurosci.* 2007;8(9):700–11.
- Biswal B, Yetkin FZ, Haughton VM, Hyde JS. Functional connectivity in the motor cortex of resting human brain using echo-planar MRI. *Magn Reson Med.* 1995;34(4):537–41.
- Cao H, Plichta MM, Schafer A, Haddad L, Grimm O, Schneider M, et al. Test-retest reliability of fMRI-based graph theoretical properties during working memory, emotion processing, and resting state. *Neuroimage.* 2014;84:888–900.
- Shehzad Z, Kelly AM, Reiss PT, Gee DG, Gotimer K, Uddin LQ, et al. The resting brain: unconstrained yet reliable. *Cereb Cortex.* 2009;19(10):2209–29.
- Ge T, Holmes AJ, Buckner RL, Smoller JW, Sabuncu MR. Heritability analysis with repeat measurements and its application to resting-state functional connectivity. *Proc Natl Acad Sci U S A.* 2017;114(21):5521–6.
- Glahn DC, Winkler AM, Kochunov P, Almasy L, Duggirala R, Carless MA, et al. Genetic control over the resting brain. *Proc Natl Acad Sci U S A.* 2010;107(3):1223–8.
- Zhang X, Xu R, Ma H, Qian Y, Zhu J. Brain structural and functional damage network localization of suicide. *Biol Psychiatry.* 2024;95(12):1091–9.
- Mo F, Zhao H, Li Y, Cai H, Song Y, Wang R, et al. Network localization of state and trait of auditory verbal hallucinations in schizophrenia. *Schizophr Bull.* 2024.
- Cheng Y, Cai H, Liu S, Yang Y, Pan S, Zhang Y, et al. Brain Network Localization of Gray Matter Atrophy and Neurocognitive and Social Cognitive Dysfunction in Schizophrenia. *Biol Psychiatry.* 2024.
- Cai H, Wang C, Qian Y, Zhang S, Zhang C, Zhao W, et al. Large-scale functional network connectivity mediate the associations of gut microbiota with sleep quality and executive functions. *Hum Brain Mapp.* 2021;42(10):3088–101.
- Tomasi D, Volkow ND. Functional connectivity density mapping. *Proc Natl Acad Sci U S A.* 2010;107(21):9885–90.
- Tomasi D, Volkow ND. Association between functional connectivity hubs and brain networks. *Cereb Cortex.* 2011;21(9):2003–13.
- Liu X, Zhao Y, Suo X, Zhang X, Pan N, Kemp GJ, et al. Psychological resilience mediates the protective role of default-mode network functional connectivity against COVID-19 vicarious traumatization. *Transl Psychiatry.* 2023;13(1):231.
- Tomasi D, Shokri-Kojori E, Volkow ND. High-resolution functional connectivity density: hub locations, sensitivity, specificity, reproducibility, and reliability. *Cereb Cortex.* 2016;26(7):3249–59.
- Tomasi D, Volkow ND. Abnormal functional connectivity in children with attention-deficit/hyperactivity disorder. *Biol Psychiatry.* 2012;71(5):443–50.
- Zhao W, Zhu DM, Li S, Cui S, Jiang P, Wang R, et al. The reduction of vitamin D in females with major depressive disorder is associated with worse cognition mediated by abnormal brain functional connectivity. *Prog Neuropsychopharmacol Biol Psychiatry.* 2022;118: 110577.
- Liu H, Yu H, Li Y, Qin W, Xu L, Yu C, et al. An energy-efficient intrinsic functional organization of human working memory: A resting-state functional connectivity study. *Behav Brain Res.* 2017;316:66–73.
- Xu Q, Liu F, Qin W, Jiang T, Yu C. Multiscale neurobiological correlates of human neuroticism. *Hum Brain Mapp.* 2020;41(16):4730–43.
- Cui S, Jiang P, Cheng Y, Cai H, Zhu J, Yu Y. Molecular mechanisms underlying resting-state brain functional connectivity of behavioral inhibition. *Neuroimage.* 2023;283: 120415.
- Hawrylycz MJ, Lein ES, Guillozet-Bongaarts AL, Shen EH, Ng L, Miller JA, et al. An anatomically comprehensive atlas of the adult human brain transcriptome. *Nature.* 2012;489(7416):391–9.
- Shen EH, Overly CC, Jones AR. The Allen Human Brain Atlas: comprehensive gene expression mapping of the human brain. *Trends Neurosci.* 2012;35(12):711–4.
- Arnatkeviciute A, Fulcher BD, Fornito A. A practical guide to linking brain-wide gene expression and neuroimaging data. *Neuroimage.* 2019;189:353–67.
- Fornito A, Arnatkeviciute A, Fulcher BD. Bridging the gap between connectome and transcriptome. *Trends Cogn Sci.* 2019;23(1):34–50.
- Sun X, Huang W, Wang J, Xu R, Zhang X, Zhou J, et al. Cerebral blood flow changes and their genetic mechanisms in major depressive disorder: a combined neuroimaging and transcriptome study. *Psychol Med.* 2023;1–13.
- Zhao H, Cai H, Mo F, Lu Y, Yao S, Yu Y, et al. Genetic mechanisms underlying brain functional homotopy: a combined transcriptome and resting-state functional MRI study. *Cereb Cortex.* 2023;33(7):3387–400.
- Liu S, Zhang C, Meng C, Wang R, Jiang P, Cai H, et al. Frequency-dependent genetic modulation of neuronal oscillations: a combined transcriptome and resting-state functional MRI study. *Cereb Cortex.* 2022;32(22):5132–44.
- Shen Y, Zhang C, Cui S, Wang R, Cai H, Zhao W, et al. Transcriptional substrates underlying functional connectivity profiles of subregions within the human sensorimotor cortex. *Hum Brain Mapp.* 2022;43(18):5562–78.
- Chen J, Zhang C, Wang R, Jiang P, Cai H, Zhao W, et al. Molecular basis underlying functional connectivity of fusiform gyrus subregions: A transcriptome-neuroimaging spatial correlation study. *Cortex.* 2022;152:59–73.
- Zhang C, Cai H, Xu X, Li Q, Li X, Zhao W, et al. Genetic architecture underlying differential resting-state functional connectivity of subregions within the human visual cortex. *Cereb Cortex.* 2022;32(10):2063–78.
- Song Y, Wang C, Cai H, Chen J, Liu S, Zhu J, et al. Functional hierarchy of the angular gyrus and its underlying genetic architecture. *Hum Brain Mapp.* 2023;44(7):2815–28.
- Xu X, Li Q, Qian Y, Cai H, Zhang C, Zhao W, et al. Genetic mechanisms underlying gray matter volume changes in patients with drug-naive first-episode schizophrenia. *Cereb Cortex.* 2023;33(5):2328–41.
- Li Q, Xu X, Qian Y, Cai H, Zhao W, Zhu J, et al. Resting-state brain functional alterations and their genetic mechanisms in drug-naive first-episode psychosis. *Schizophrenia (Heidelb).* 2023;9(1):13.

48. Fang Q, Cai H, Jiang P, Zhao H, Song Y, Zhao W, et al. Transcriptional substrates of brain structural and functional impairments in drug-naïve first-episode patients with major depressive disorder. *J Affect Disord*. 2023;325:522–33.
49. Ashburner M, Ball CA, Blake JA, Botstein D, Butler H, Cherry JM, et al. Gene ontology: tool for the unification of biology. The Gene Ontology Consortium. *Nat Genet*. 2000;25(1):25–9.
50. Fulcher BD, Arnatkevičiute A, Fornito A. Overcoming false-positive gene-category enrichment in the analysis of spatially resolved transcriptomic brain atlas data. *Nat Commun*. 2021;12(1):2669.
51. Beliveau V, Ganz M, Feng L, Ozenne B, Hojgaard L, Fisher PM, et al. A High-Resolution In Vivo Atlas of the Human Brain's Serotonin System. *J Neurosci*. 2017;37(1):120–8.
52. Lehto J, Johansson J, Vuorilehto L, Luoto P, Arponen E, Scheinin H, et al. Sensitivity of [(11C)ORM-13070 to increased extracellular noradrenaline in the CNS - a PET study in human subjects. *Psychopharmacology*. 2015;232(21–22):4169–78.
53. Mawlawi O, Martinez D, Slifstein M, Broft A, Chatterjee R, Hwang DR, et al. Imaging human mesolimbic dopamine transmission with positron emission tomography: I. Accuracy and precision of D(2) receptor parameter measurements in ventral striatum. *J Cereb Blood Flow Metab*. 2001;21(9):1034–57.
54. McCann UD, Szabo Z, Seckin E, Rosenblatt P, Mathews WB, Ravert HT, et al. Quantitative PET studies of the serotonin transporter in MDMA users and controls using [(11C)McN5652 and [(11C)DASB. *Neuropsychopharmacology*. 2005;30(9):1741–50.
55. Smith GS, Price JC, Lopresti BJ, Huang Y, Simpson N, Holt D, et al. Test-retest variability of serotonin 5-HT2A receptor binding measured with positron emission tomography and [(18F]altanserin in the human brain. *Synapse*. 1998;30(4):380–92.
56. Hansen JY, Shafiei G, Markello RD, Smart K, Cox SML, Norgaard M, et al. Mapping neurotransmitter systems to the structural and functional organization of the human neocortex. *Nat Neurosci*. 2022;25(11):1569–81.
57. Li J, Kong XZ. Morphological connectivity correlates with trait impulsivity in healthy adults. *PeerJ*. 2017;5: e3533.
58. Herath P, Kinomura S, Roland PE. Visual recognition: evidence for two distinctive mechanisms from a PET study. *Hum Brain Mapp*. 2001;12(2):110–9.
59. Mechelli A, Gorno-Tempini ML, Price CJ. Neuroimaging studies of word and pseudoword reading: consistencies, inconsistencies, and limitations. *J Cogn Neurosci*. 2003;15(2):260–71.
60. Hamame CM, Vidal JR, Ossandon T, Jerbi K, Dalal SS, Minotti L, et al. Reading the mind's eye: online detection of visuo-spatial working memory and visual imagery in the inferior temporal lobe. *Neuroimage*. 2012;59(1):872–9.
61. Smith EE, Jonides J, Koeppe RA. Dissociating verbal and spatial working memory using PET. *Cereb Cortex*. 1996;6(1):11–20.
62. Hu Z, Samuel IBH, Meyyappan S, Bo K, Rana C, Ding M. Aftereffects of frontoparietal theta tACS on verbal working memory: Behavioral and neurophysiological analysis. *IBRO Neurosci Rep*. 2022;13:469–77.
63. Nagel BJ, Herting MM, Maxwell EC, Bruno R, Fair D. Hemispheric lateralization of verbal and spatial working memory during adolescence. *Brain Cogn*. 2013;82(1):58–68.
64. Arabaci G, Cakir BS, Parris BA. The effect of high-frequency rTMS over left DLPFC and fluid abilities on goal neglect. *Brain Struct Funct*. 2024;229(5):1073–86.
65. Zhang H, Feng Z, Zang Y, Zhang Y. Hemispheric lateralization and top-down regulation of the prefrontal cortex on sequential memory of familiar faces. *Annu Int Conf IEEE Eng Med Biol Soc*. 2023;2023:1–4.
66. Miller EK, Lundqvist M, Bastos AM. Working Memory 2.0. *Neuron*. 2018;100(2):463–75.
67. Rutishauser U, Reddy L, Mormann F, Sarnthein J. The architecture of human memory: insights from human single-neuron recordings. *J Neurosci*. 2021;41(5):883–90.
68. Mu L, Cai J, Gu B, Yu L, Li C, Liu QS, et al. Treadmill exercise prevents decline in spatial learning and Memory in 3xTg-AD mice through enhancement of structural synaptic plasticity of the hippocampus and prefrontal Cortex. *Cells*. 2022;11(2):244.
69. Chung S, Fieremans E, Kucukboyaci NE, Wang X, Morton CJ, Novikov DS, et al. Working memory and brain tissue microstructure: white matter tract integrity based on multi-shell diffusion MRI. *Sci Rep*. 2018;8(1):3175.
70. Coltman R, Spain A, Tsenkina Y, Fowler JH, Smith J, Scullion G, et al. Selective white matter pathology induces a specific impairment in spatial working memory. *Neurobiol Aging*. 2011;32(12):2324 e7-12.
71. Goldman-Rakic PS. Cellular basis of working memory. *Neuron*. 1995;14(3):477–85.
72. Silvano J. Working memory maintenance: sustained firing or synaptic mechanisms? *Trends Cogn Sci*. 2017;21(3):152–4.
73. Yamamoto J, Suh J, Takeuchi D, Tonegawa S. Successful execution of working memory linked to synchronized high-frequency gamma oscillations. *Cell*. 2014;157(4):845–57.
74. Sreenivasan KK, Curtis CE, D'Esposito M. Revisiting the role of persistent neural activity during working memory. *Trends Cogn Sci*. 2014;18(2):82–9.
75. Manohar SG, Zokaei N, Fallon SJ, Vogels TP, Husain M. Neural mechanisms of attending to items in working memory. *Neurosci Biobehav Rev*. 2019;101:1–12.
76. Barnett SC, Parr-Brownlie LC, Perry BAL, Young CK, Wicky HE, Hughes SM, et al. Anterior thalamic nuclei neurons sustain memory. *Curr Res Neurobiol*. 2021;2:100022.
77. Roy DS, Zhang Y, Aida T, Shen C, Skaggs KM, Hou Y, et al. Anterior thalamic circuits crucial for working memory. *Proc Natl Acad Sci U S A*. 2022;119(20): e2118712119.
78. Catterall WA. From ionic currents to molecular mechanisms: the structure and function of voltage-gated sodium channels. *Neuron*. 2000;26(1):13–25.
79. Haldane M, Jogia J, Cobb A, Kozuch E, Kumari V, Frangou S. Changes in brain activation during working memory and facial recognition tasks in patients with bipolar disorder with Lamotrigine monotherapy. *Eur Neuropsychopharmacol*. 2008;18(1):48–54.
80. Takahashi H, Yamada M, Suhara T. Functional significance of central D1 receptors in cognition: beyond working memory. *J Cereb Blood Flow Metab*. 2012;32(7):1248–58.
81. Luciana M, Depue RA, Arbsi P, Leon A. Facilitation of working memory in humans by a d2 dopamine receptor agonist. *J Cogn Neurosci*. 1992;4(1):58–68.
82. D'Esposito M, Postle BR. The cognitive neuroscience of working memory. *Annu Rev Psychol*. 2015;66:115–42.
83. O'Reilly RC. Biologically based computational models of high-level cognition. *Science*. 2006;314(5796):91–4.
84. Wang M, Vijayraghavan S, Goldman-Rakic PS. Selective D2 receptor actions on the functional circuitry of working memory. *Science*. 2004;303(5659):853–6.
85. Glickstein SB, Hof PR, Schmauss C. Mice lacking dopamine D2 and D3 receptors have spatial working memory deficits. *J Neurosci*. 2002;22(13):5619–29.
86. Niswender CM, Conn PJ. Metabotropic glutamate receptors: physiology, pharmacology, and disease. *Annu Rev Pharmacol Toxicol*. 2010;50:295–322.
87. Yang ST, Wang M, Galvin V, Yang Y, Arnsten AFT. Effects of blocking mGluR5 on primate dorsolateral prefrontal cortical neuronal firing and working memory performance. *Psychopharmacology*. 2021;238(1):97–106.
88. Meneses A, Terron JA, Hong E. Effects of the 5-HT receptor antagonists GR127935 (5-HT1B/1D) and MDL100907 (5-HT2A) in the consolidation of learning. *Behav Brain Res*. 1997;89(1–2):217–23.
89. Roth BL, Hanizavareh SM, Blum AE. Serotonin receptors represent highly favorable molecular targets for cognitive enhancement in schizophrenia and other disorders. *Psychopharmacology*. 2004;174(1):17–24.
90. Bartus RT, Dean RL 3rd, Beer B, Lippa AS. The cholinergic hypothesis of geriatric memory dysfunction. *Science*. 1982;217(4558):408–14.
91. Al-Onaizi MA, Parfitt GM, Kolisnyk B, Law CS, Guzman MS, Barros DM, et al. Regulation of Cognitive Processing by Hippocampal Cholinergic Tone. *Cereb Cortex*. 2017;27(2):1615–28.
92. Iversen SD. Behavioural evaluation of cholinergic drugs. *Life Sci*. 1997;60(13–14):1145–52.
93. Seeger T, Fedorova I, Zheng F, Miyakawa T, Koustova E, Gomeza J, et al. M2 muscarinic acetylcholine receptor knock-out mice show deficits in behavioral flexibility, working memory, and hippocampal plasticity. *J Neurosci*. 2004;24(45):10117–27.

94. E-Prime. 2002. <http://www.psnet.com/eprime.cfm>.
95. Friston K, Ashburner J, Heather J, Holmes A, Poline JB. Statistical Parametric Mapping. 2014. <http://www.fil.ion.ucl.ac.uk/spm>.
96. Yan CG, Wang XD, Zuo XN, Zang YF. DPABI: Data Processing & Analysis for (Resting-State) Brain Imaging. *Neuroinformatics*. 2016;14(3):339–51.
97. Yan CG, Wang XD, Zuo XN, Zang YF. DPABI: a toolbox for Data Processing & Analysis for Brain Imaging. 2016. <http://rfmri.org/dpabi>.
98. Murphy K, Fox MD. Towards a consensus regarding global signal regression for resting state functional connectivity MRI. *Neuroimage*. 2017;154:169–73.
99. Ashburner J. A fast diffeomorphic image registration algorithm. *Neuroimage*. 2007;38(1):95–113.
100. Zhuo C, Wang C, Wang L, Guo X, Xu Q, Liu Y, et al. Altered resting-state functional connectivity of the cerebellum in schizophrenia. *Brain Imaging Behav*. 2018;12(2):383–9.
101. Zhuo C, Zhu J, Qin W, Qu H, Ma X, Tian H, et al. Functional connectivity density alterations in schizophrenia. *Front Behav Neurosci*. 2014;8:404.
102. Zhu J, Wang C, Qian Y, Cai H, Zhang S, Zhang C, et al. Multimodal neuroimaging fusion biomarkers mediate the association between gut microbiota and cognition. *Prog Neuropsychopharmacol Biol Psychiatry*. 2022;113: 110468.
103. Buckner RL, Sepulcre J, Talukdar T, Krienen FM, Liu H, Hedden T, et al. Cortical hubs revealed by intrinsic functional connectivity: mapping, assessment of stability, and relation to Alzheimer's disease. *J Neurosci*. 2009;29(6):1860–73.
104. Wang Y, Kwapong WR, Tu Y, Xia Y, Tang J, Miao H, et al. Altered resting-state functional connectivity density in patients with neuromyelitis optica-spectrum disorders. *Mult Scler Relat Disord*. 2020;43: 102187.
105. Zhou F, Zhu Y, Zhu Y, Huang M, Jiang J, He L, et al. Altered long- and short-range functional connectivity density associated with poor sleep quality in patients with chronic insomnia disorder: A resting-state fMRI study. *Brain Behav*. 2020;10(11): e01844.
106. Allen Brain Map. 2003. <http://www.brain-map.org>.
107. Arloth J, Bader DM, Roh S, Altmann A. Re-annotator: annotation pipeline for microarray probe sequences. *PLoS ONE*. 2015;10(10): e0139516.
108. Xie Y, Zhang X, Liu F, Qin W, Fu J, Xue K, et al. Brain mRNA expression associated with cortical volume alterations in autism spectrum disorder. *Cell Rep*. 2020;32(11): 108137.
109. Kang HJ, Kawasawa YI, Cheng F, Zhu Y, Xu X, Li M, et al. Spatio-temporal transcriptome of the human brain. *Nature*. 2011;478(7370):483–9.
110. Hawrylycz M, Miller JA, Menon V, Feng D, Dolbeare T, Guillozet-Bongaerts AL, et al. Canonical genetic signatures of the adult human brain. *Nat Neurosci*. 2015;18(12):1832–44.
111. Fan L, Li H, Zhuo J, Zhang Y, Wang J, Chen L, et al. The human brain-netome atlas: a new brain atlas based on connectonal architecture. *Cereb Cortex*. 2016;26(8):3508–26.
112. Gene Ontology. <https://doi.org/10.5281/zenodo.1205166>. Accessed 11 Jul 2022.
113. Burt JB, Helmer M, Shinn M, Anticevic A, Murray JD. BrainSMASH. 2020. <https://github.com/murraylab/brainsmash>.
114. Burt JB, Helmer M, Shinn M, Anticevic A, Murray JD. Generative modeling of brain maps with spatial autocorrelation. *Neuroimage*. 2020;220: 117038.
115. Dukart J, Holiga S, Rullmann M, Lanzenberger R, Hawkins PCT, Mehta MA, et al. JuSpace. 2020. <https://github.com/juryxy/JuSpace>.
116. Dukart J, Holiga S, Rullmann M, Lanzenberger R, Hawkins PCT, Mehta MA, et al. JuSpace: A tool for spatial correlation analyses of magnetic resonance imaging data with nuclear imaging derived neurotransmitter maps. *Hum Brain Mapp*. 2021;42(3):555–66.
117. Savli M, Bauer A, Mitterhauser M, Ding YS, Hahn A, Kroll T, et al. Normative database of the serotonergic system in healthy subjects using multi-tracer PET. *Neuroimage*. 2012;63(1):447–59.
118. Normandin MD, Zheng MQ, Lin KS, Mason NS, Lin SF, Ropchan J, et al. Imaging the cannabinoid CB1 receptor in humans with [11C]OMAR: assessment of kinetic analysis methods, test-retest reproducibility, and gender differences. *J Cereb Blood Flow Metab*. 2015;35(8):1313–22.
119. Kaller S, Rullmann M, Patt M, Becker GA, Luthardt J, Girbardt J, et al. Test-retest measurements of dopamine D1-type receptors using simultaneous PET/MRI imaging. *Eur J Nucl Med Mol Imaging*. 2017;44(6):1025–32.
120. Alakurtti K, Johansson JJ, Joutsa J, Laine M, Backman L, Nyberg L, et al. Long-term test-retest reliability of striatal and extrastriatal dopamine D2/3 receptor binding: study with [(11C)raclopride and high-resolution PET. *J Cereb Blood Flow Metab*. 2015;35(7):1199–205.
121. Zakiniaieiz Y, Hillmer AT, Matuskey D, Nabulsi N, Ropchan J, Mazure CM, et al. Sex differences in amphetamine-induced dopamine release in the dorsolateral prefrontal cortex of tobacco smokers. *Neuropsychopharmacology*. 2019;44(13):2205–11.
122. Dukart J, Holiga S, Chatham C, Hawkins P, Forsyth A, McMillan R, et al. Cerebral blood flow predicts differential neurotransmitter activity. *Sci Rep*. 2018;8(1):4074.
123. Garcia-Gomez FJ, Garcia-Solis D, Luis-Simon FJ, Marin-Oyaga VA, Carrillo F, Mir P, et al. Elaboración de una plantilla de SPM para la normalización de imágenes de SPECT con 123I-Ioflupano. *Rev Esp Med Nucl Imagen Mol*. 2013;32(6):350–6.
124. Norgaard M, Beliveau V, Ganz M, Svarer C, Pinborg LH, Keller SH, et al. A high-resolution in vivo atlas of the human brain's benzodiazepine binding site of GABAA receptors. *Neuroimage*. 2021;232:117878.
125. Kantonen T, Karjalainen T, Isojarvi J, Nuutila P, Tuisku J, Rinne J, et al. Interindividual variability and lateralization of mu-opioid receptors in the human brain. *Neuroimage*. 2020;217: 116922.
126. Turttonen O, Saarinen A, Nummenmaa L, Tuominen L, Tikka M, Armio RL, et al. Adult Attachment System Links With Brain Mu Opioid Receptor Availability In Vivo. *Biol Psychiatry Cogn Neurosci Neuroimaging*. 2021;6(3):360–9.
127. Hesse S, Becker GA, Rullmann M, Bresch A, Luthardt J, Hankir MK, et al. Central noradrenaline transporter availability in highly obese, non-depressed individuals. *Eur J Nucl Med Mol Imaging*. 2017;44(6):1056–64.
128. Aghourian M, Legault-Denis C, Soucy JP, Rosa-Neto P, Gauthier S, Kostikov A, et al. Quantification of brain cholinergic denervation in Alzheimer's disease using PET imaging with [(18F)-FEOBV. *Mol Psychiatry*. 2017;22(11):1531–8.
129. Bedard MA, Aghourian M, Legault-Denis C, Postuma RB, Soucy JP, Gagnon JF, et al. Brain cholinergic alterations in idiopathic REM sleep behaviour disorder: a PET imaging study with (18F)-FEOBV. *Sleep Med*. 2019;58:35–41.
130. DuBois JM, Rousset OG, Rowley J, Porras-Betancourt M, Reader AJ, Labbe A, et al. Characterization of age/sex and the regional distribution of mGluR5 availability in the healthy human brain measured by high-resolution [(11C)ABP688 PET. *Eur J Nucl Med Mol Imaging*. 2016;43(1):152–62.
131. Smart K, Cox SML, Scala SG, Tippler M, Jaworska N, Boivin M, et al. Sex differences in [(11C)ABP688 binding: a positron emission tomography study of mGlu5 receptors. *Eur J Nucl Med Mol Imaging*. 2019;46(5):1179–83.
132. Xu X. Molecular mechanisms underlying the neural correlates of working memory. 2024. <https://doi.org/10.17605/OSF.IO/FQ8Z3>.

## Publisher's Note

Springer Nature remains neutral with regard to jurisdictional claims in published maps and institutional affiliations.